J. Fluid Mech. (2002), *vol.* 467, *pp.* 81–100.
DOI: 10.1017/S0022112002001416 Printed in the United Kingdom

Two-dimensional cascades and mixing: a physical space approach

By THOMAS DUBOS AND ARMANDO BABIANO

Laboratoire de Météorologie Dynamique, École Normale Supérieure 24 rue Lhomond, 75231 Paris Cedex, France

(Received 16 November 2001 and in revised form 23 March 2002)

We develop an analysis of the two-dimensional cascade of a tracer (passive or active Lagrangian-conserved scalar), locally in space and time, and establish connections with the modelling of turbulent mixing. We define a local scale-to-scale flux of tracer variance based on the dynamics of tracer increments. This flux reduces at small scales to the production or destruction rate of tracer gradients by stirring as a function of their local orientation with respect to the compressional axis of the strain-rate tensor. The local detailed budget of tracer variance on which this approach is based is compared to the global statistical budget expressed by Yaglom's equation. The spatial pattern of the local transfers produced by a numerical simulation as well as their statistical distribution are discussed.

We then address the problem of the parameterization of turbulent mixing. We consider an anisotropic tensor diffusivity proportional to the velocity gradients. In this model the tracer dissipation involves the axes of the strain-rate tensor and we shall refer to it as *strain diffusivity*. We show analytically that it locally matches the scale-to-scale flux through the cutoff scale. This matching is studied numerically in decaying two-dimensional turbulence. A comparison is made with eddy diffusivity and hyperdiffusivity. The presence of a numerical instability and ways to suppress it are discussed from numerical and fundamental points of view.

We consider the special case of vorticity, an active scalar in two dimensions. When applied to vorticity, models affect the energy budget. The two-dimensional inverse energy cascade requires that parameterizations conserve energy and we show that strain diffusivity conserves energy. We finally study the sensitivity of the large scales of the flow to the operator used on vorticity in forced stationary simulations. Strain diffusivity is found to produce more realistic spectral features than hyperviscosity.

1. Introduction

Mixing is a fundamental process involved in the transport properties of flows, and especially of turbulent flows. In this respect, two-dimensional turbulent mixing is of special interest, both for its theoretical originality and because it is a good conceptual basis from which to understand the transport and mixing properties of geophysical flows (Pedlosky 1979; Rhines 1979). From a Lagrangian viewpoint, mixing is related to the process by which two initially separated particles come very close to each other (Crisanti *et al.* 1990). From a Eulerian viewpoint, the signature of mixing is a decrease of the variance of the tracer field. In terms of a turbulent cascade in Fourier space in the sense of Obukhov–Corrsin–Batchelor theory (Obukhov 1949; Corrsin 1951; Batchelor 1959), the tracer variance is transferred from small wavenumbers to high

wavenumbers by the stirring action of the advecting flow that creates smaller and smaller scales of the tracer field. Due to the resulting spectral flux of tracer variance, the tracer variance contained in any bounded domain of wavenumbers decreases. As a consequence, in a Eulerian observation with finite resolution, the conserved quantity carried by two particles that approach each other is averaged over the resolved scale, resulting in an irreversible loss of information. Now, even if the cascade stops at some finite wavenumber due to a non-zero molecular diffusivity, this diffusive scale is often unreachable in direct numerical simulations. Thus from a practical point of view, limitations on resolution imply that the mixing process must be parameterized introducing in the advection equation artificial terms designed to destroy the resolved tracer variance. This is often done using an *ad hoc* eddy diffusivity, in analogy with molecular diffusivity (Smagorinsky 1963).

It is well established in the theory of geophysical fluid dynamics that molecular diffusion usually acts at scales much smaller than required by the two-dimensional assumption. Therefore the two-dimensional Laplacian operator, although often considered more physical, is actually an eddy diffusivity, a parameterization among the various available ones. Many parameterizations such as eddy diffusivity and hyperdiffusivity (Basdevant *et al.* 1981) essentially rely on the very successful concept of a turbulent cascade in Fourier space. However Fourier analysis merely deals with amplitudes and spatial averages, missing the geometry and local details of the flow which might be relevant. This was a motivation for recent work focusing on the physical space properties of the cascade. Much progress has been made recently in this area, mainly in the analysis of the two-dimensional tracer gradient dynamics and especially the dynamics of its orientation (Weiss 1991; Basdevant & Philipovitch 1994; Hua & Klein 1998; Protas, Babiano & Kevlahan 1999; Lapeyre, Klein & Hua 1999; Klein, Hua & Lapeyre 2000). One main conclusion of these studies is that the cascade process is locally strongly anisotropic since tracer gradients tend to align with preferred directions. This justifies further exploration of some of the mixing properties of two-dimensional turbulence using an analysis based on the real space cascade process.

The main purpose of this paper is to develop an analysis of the two-dimensional tracer cascade, locally in space and time, and establish connections with the modelling of turbulent mixing. We define a local scale-to-scale flux of tracer variance based on the dynamics of tracer increments. This flux reduces at small scales to the production or destruction rate of tracer gradients by stirring as a function of its local orientation with respect to the compressional axis of the strain-rate tensor. The local detailed budget of tracer variance on which this approach is based is compared to the global statistical budget expressed by Yaglom's equation (Yaglom 1949). The spatial pattern of the local transfers produced by a numerical simulation as well as their statistical distribution are discussed. We then address the problem of the parameterization of turbulent mixing. We consider an anisotropic tensor diffusivity proportional to the velocity gradients. In this model the tracer dissipation involves the axes of the strain-rate tensor and we shall refer to it as *strain diffusivity*. We show analytically that it locally matches the scale-to-scale flux through the cutoff scale. This matching is studied numerically in decaying two-dimensional turbulence. A comparison is made with isotropic eddy diffusivity and hyperdiffusivity. We finally consider the special case of vorticity, an active tracer in two dimensions. When applied to vorticity, models affect the energy budget. The two-dimensional inverse energy cascade (Kraichnan 1967; Paret & Tabeling 1997; Boffetta, Celani & Vergassola 2000; Dubos *et al.* 2001) requires that parameterizations conserve the total energy (Basdevant *et al.* 1981) and

we show that strain diffusivity conserves energy. We finally study the sensitivity of the large scales of the flow to the operator used on vorticity in simulations of forced stationary two-dimensional turbulence.

The paper is organized as follows. In § 2 we develop the analysis of the tracer cascade based on the dynamics of tracer increments. In § 3 we address the problem of the parameterization of turbulent mixing. Section 4 is devoted to the particular case of two-dimensional vorticity. The conclusions are summarized and discussed in § 5.

2. Tracer cascade in physical space

Let us first recall the basic concept of the turbulent cascade in spectral space (Corrsin 1951; Batchelor 1959; Kraichnan 1971). It is based on the evolution of the one-dimensional tracer spectrum $Z_T(k)$ in a forced and dissipated situation:

$$\frac{\partial Z_T(k)}{\partial t} + \frac{\partial \eta_T}{\partial k} = P_T(k) - \kappa k^2 Z_T(k), \tag{2.1}$$

$$Z_T(k) \equiv \frac{1}{2} \int_{\|\boldsymbol{k}\|=k} |T(\boldsymbol{k})|^2 \, \mathrm{d}\boldsymbol{k}, \tag{2.2}$$

$$\eta_T(k) \equiv \int_{\|\boldsymbol{k}\|<k} T(\boldsymbol{k}) \cdot n_T^*(\boldsymbol{k}), \tag{2.3}$$

where $T(\boldsymbol{k})$ is the Fourier representation of the tracer field $T(\boldsymbol{x})$, κ the molecular diffusivity, $P_T(k)$ the variance input by forcing, $\eta_T(k)$ the spectral flux of tracer variance and $n_T(\boldsymbol{x}) \equiv (\boldsymbol{u} \cdot \nabla) T$ the convective term of the forced advection–diffusion equation:

$$\frac{\partial T}{\partial t} + (\boldsymbol{u} \cdot \nabla)\, T = \kappa \Delta T + f_T, \tag{2.4}$$

with $\boldsymbol{u}(\boldsymbol{x})$ the advecting velocity field and $f_T(\boldsymbol{x})$ the forcing.

The quadratic quantity associated with T is its variance $Z_T = \int_0^\infty Z(k)\, \mathrm{d}k = \int \frac{1}{2} T^2 \, \mathrm{d}\boldsymbol{x}/V$ with V the volume (area) occupied by the fluid. The spectral picture of the tracer cascade is then as follows. The forcing f_T creates large-scale patches of tracer and inputs variance at a rate $P_T(k)$. The stretching and folding action of the advecting field creates structures (like filaments or fronts) of smaller and smaller scale. Thus the stirring globally conserves the tracer variance and transfers it from large scales (small wavenumbers) to small scales (high wavenumbers), at a rate measured by the spectral flux $\eta_T(k)$ which is expected to be directed towards small scales (positive). When the transferred variance reaches a sufficiently small scale, the homogenizing action of diffusion ultimately destroys it. But the existence of the cascade itself is a convective process that takes place even in the absence of forcing and diffusion.

2.1. *Dynamics of tracer increments*

We develop an alternative picture of the cascade through the dynamics of tracer increments. Indeed, structures of scale l can be detected through the magnitude of the tracer difference over the distance l. We first focus for simplicity on the advection terms of equation (2.4) then discuss the effect of forcing and diffusion in connection with Yaglom's equation. We finally consider the small-scale limit.

Local flux of tracer variance

We consider the tracer increment $\delta T(\boldsymbol{x},\boldsymbol{l})$ at position $\boldsymbol{x}$ and vector separation $\boldsymbol{l}$ defined by $\delta T \equiv T^+ - T^-$ where $T^{\pm}(\boldsymbol{x},\boldsymbol{l}) \equiv T(\boldsymbol{x} \pm \boldsymbol{l}/2)$, and more specifically its magnitude measured by δT^2. Both δT and δT^2 are functions of the two vectors $\boldsymbol{x}$ and $\boldsymbol{l}$ and obey in the present non-forced non-diffusive context:

$$\left(\frac{\partial}{\partial t} + \boldsymbol{u}^{\pm}\cdot\nabla\right) T^{\pm} = 0,$$

$$\left(\frac{\partial}{\partial t} + \boldsymbol{U}\cdot\nabla\right) \delta T = -\frac{\delta\boldsymbol{u}}{2}\cdot\nabla(T^+ + T^-),$$

where we have introduced the velocity increment $\delta\boldsymbol{u} \equiv \boldsymbol{u}^+ - \boldsymbol{u}^-$ and the pair-averaged velocity $\boldsymbol{U} \equiv (\boldsymbol{u}^+ + \boldsymbol{u}^-)/2$, with $\boldsymbol{u}^{\pm}(\boldsymbol{x},\boldsymbol{l}) \equiv \boldsymbol{u}(\boldsymbol{x} \pm \boldsymbol{l}/2)$. Taking advantage of the relations between derivatives in $\boldsymbol{x}$ and $\boldsymbol{l}$ ($2\nabla_{\boldsymbol{l}} T^{\pm} = \pm\nabla_{\boldsymbol{x}} T^{\pm}$), we transform this equation into

$$\left(\frac{\partial}{\partial t} + \boldsymbol{U}\cdot\nabla_{\boldsymbol{x}} + \delta\boldsymbol{u}\cdot\nabla_{\boldsymbol{l}}\right) \delta T = 0, \tag{2.5}$$

$$\left(\frac{\partial}{\partial t} + \boldsymbol{U}\cdot\nabla_{\boldsymbol{x}} + \delta\boldsymbol{u}\cdot\nabla_{\boldsymbol{l}}\right) \delta T^2 = 0. \tag{2.6}$$

Equation (2.6) is obtained by multiplying (2.5) by $2\delta T$.

The form of the evolution equations of δT and δT^2 is familiar: they are transport equations in the four-dimensional space $(\boldsymbol{x},\boldsymbol{l})$. So while the tracer is transported in physical space, its increment δT and its square δT^2 are transported both in physical space at velocity $\boldsymbol{U}(\boldsymbol{x},\boldsymbol{l})$ and through scales at velocity $\delta\boldsymbol{u}(\boldsymbol{x},\boldsymbol{l})$. This interpretation gives a simple picture of the scale-to-scale cascade.

The scale of a structure is a scalar l rather than a vector $\boldsymbol{l}$. Thus we need to integrate over the angular component ϕ of $\boldsymbol{l}$. We do this by expressing (2.6) in polar coordinates (l,ϕ) for $\boldsymbol{l}$. First, using the incompressibility of $\delta\boldsymbol{u}$ with respect to $\boldsymbol{l}$ ($\nabla_{\boldsymbol{l}}\cdot\delta\boldsymbol{u} = 0$) the gradients in (2.6) become divergences of fluxes:

$$\frac{\partial}{\partial t}\delta T^2 + \nabla_{\boldsymbol{x}}\cdot(\delta T^2\boldsymbol{U}) + \nabla_{\boldsymbol{l}}\cdot(\delta T^2\delta\boldsymbol{u}) = 0. \tag{2.7}$$

In polar coordinates, the radial and azimuthal components of the velocity increment are respectively its longitudinal component $\delta u_{\parallel} \equiv \boldsymbol{l}/l\cdot\delta\boldsymbol{u}$ and its transverse component $\delta u_{\perp} \equiv (\boldsymbol{l}/l \times \delta\boldsymbol{u})\cdot\boldsymbol{e}_z$, with $\boldsymbol{e}_z$ a unit vector orthogonal to the flow plane:

$$\frac{\partial}{\partial t}\delta T^2 + \nabla_{\boldsymbol{x}}\cdot(\delta T^2\boldsymbol{U}) + \frac{\partial}{l\partial l}(l\delta T^2\delta u_{\parallel}) + \frac{\partial}{l\partial\phi}(\delta T^2\delta u_{\perp}) = 0.$$

Integrating over the azimuthal angle ϕ we obtain

$$\frac{\partial}{\partial t}\oint \delta T^2\frac{\mathrm{d}\phi}{2\pi} + \nabla_{\boldsymbol{x}}\cdot\oint \delta T^2\boldsymbol{U}\frac{\mathrm{d}\phi}{2\pi} + \frac{\partial}{l\partial l}l\oint \delta T^2\delta u_{\parallel}\frac{\mathrm{d}\phi}{2\pi} = 0. \tag{2.8}$$

As in (2.6), the time evolution of $\oint \delta T^2\mathrm{d}\phi/2\pi$ results from two contributions: on one hand a transport in physical space expressed by the $\boldsymbol{x}$-divergence of the flux $\oint \delta T^2\boldsymbol{U}\mathrm{d}\phi/2\pi$; on the other hand a transfer from scale to scale expressed by the last term of (2.8). The flux $\oint \delta T^2\delta u_{\parallel}\mathrm{d}\phi/2\pi$ is directed towards large scales since the corresponding divergence is over l. In order to obtain a flux towards small scales that has the dimension of the spectral flux $\eta_T(k)$, we define $F(\boldsymbol{x},l)$, the local flux of tracer

variance from scales larger than l to scales smaller than l as

$$F(\boldsymbol{x},l) \equiv -\frac{1}{2l}\oint \delta u_{\parallel}(\boldsymbol{x},l,\phi)\delta T^2(\boldsymbol{x},l,\phi)\frac{\mathrm{d}\phi}{2\pi}$$
$$= -\frac{1}{2l}\left\langle \delta u_{\parallel}\delta T^2\right\rangle_{\phi}, \tag{2.9}$$

where the brackets $\langle\,\rangle$ indicate an average over the variable specified as index, here ϕ.

Connection with Yaglom's equation

We now consider the full equation (2.4). In the presence of forcing and diffusion, the budget equation (2.7) becomes (see Appendix A)

$$\left(\frac{\partial}{\partial t} + \boldsymbol{U}\cdot\nabla_{\boldsymbol{x}} + \delta\boldsymbol{u}\cdot\nabla_{\boldsymbol{l}} - \kappa(\tfrac{1}{2}\,\Delta_{\boldsymbol{x}} + 2\,\Delta_{\boldsymbol{l}})\right)\frac{\delta T^2}{2} = \delta T\delta f_T - (\eta_T^+ + \eta_T^-), \tag{2.10}$$

with $\eta_T(\boldsymbol{x}) \equiv \kappa\,\|\nabla_{\boldsymbol{x}} T\|^2$ and $\eta_T^{\pm} \equiv \eta_T(\boldsymbol{x} \pm \boldsymbol{l}/2)$. In such a forced and dissipated case, a statistically stationary state may be reached. In this case we obtain, on expressing the operators $\nabla_{\boldsymbol{l}}$ and $\Delta_{\boldsymbol{l}}$ in polar coordinates (l,ϕ) then averaging over the angle ϕ, the position $\boldsymbol{x}$ and the time t:

$$\frac{\mathrm{d}}{l\,\mathrm{d}l}l\langle\delta T^2\delta u_{\parallel}\rangle_{x,t,\phi} - \frac{\kappa}{2l}\frac{\mathrm{d}}{\mathrm{d}l}l\frac{\mathrm{d}}{\mathrm{d}l}\langle\delta T^2\rangle_{x,t,\phi} = 2\langle\delta T\delta f_T\rangle_{x,t,\phi} - 4\langle\eta_T\rangle_{x,t}.$$

At a scale much smaller than the typical forcing scale, the forcing power $\langle\delta T\delta f_T\rangle_{x,t,\phi}$ can be neglected so that (after integrating over l) we recover the two-dimensional Yaglom equation (Yaglom 1949):

$$\langle\delta T^2\delta u_{\parallel}\rangle_{x,t,\phi} + 2l\langle\eta_T\rangle_{x,t} = 2\kappa\frac{\mathrm{d}}{\mathrm{d}l}\langle\delta T^2\rangle_{x,t,\phi}. \tag{2.11}$$

At convective scales l, the last diffusive term is negligible (Monin & Yaglom 1971) and equation (2.11) further reduces to a balance between the flux $F(\boldsymbol{x},l)$ due to differential advection and tracer inhomogeneity (equation (2.9)) and destruction by diffusion:

$$\langle F(\boldsymbol{x},l)\rangle_{x,t} = \langle\eta_T\rangle_{x,t}. \tag{2.12}$$

Yaglom's equation (2.12) expresses a global statistical balance between the stirring that turns large-scale tracer patches into small-scale structures and diffusion that destroys the latter. What we have shown here is that this balance can be made meaningful locally in time and space for a single realization of the flow and tracer field via the budget equations (2.8) and (2.10). This dynamical balance defines the local flux $F(\boldsymbol{x},l)$ by equation (2.9).

2.2. *Small-scale limit: dynamics of tracer gradients*

If we consider a scale at which the tracer and velocity fields are smooth (which is true in particular for the velocity field in the direct enstrophy cascade range (Babiano, Basdevant & Sadourny 1985), a Taylor expansion of equation (2.9) leads to

$$F(\boldsymbol{x},l) \approx -\frac{l^2}{4}\partial_i T\partial_i u_j\partial_j T. \tag{2.13}$$

The right-hand side of equation (2.13) is directly related to the growth of the tracer gradients. This growth process is described by the Lagrangian evolution of the norm

of the tracer gradient $\boldsymbol{q} = \nabla T$, obtained by taking the gradient of equation (2.4). Focusing on the convective terms, one obtains

$$\left.\frac{\mathrm{d}\boldsymbol{q}}{\mathrm{d}t}\right|_{stirring} = -\boldsymbol{A}^T\boldsymbol{q}, \tag{2.14}$$

$$\left.\frac{\mathrm{d}\boldsymbol{q}^2}{\mathrm{d}t}\right|_{stirring} = -\boldsymbol{q}^T\boldsymbol{S}\boldsymbol{q} = -2\partial_i T\partial_i u_j \partial_j T, \tag{2.15}$$

with $A_{ij} = \partial_j u_i$ the velocity gradient, $\boldsymbol{A}^T$ its transpose and $S_{ij} = \partial_j u_i + \partial_i u_j$ the strain-rate tensor (symmetric part of $\boldsymbol{A}$). This tensor $\boldsymbol{S}$ involved in the tracer gradient production rate $-\boldsymbol{q}^T\boldsymbol{S}\boldsymbol{q}$ is traceless due to incompressibility and has two opposite eigenvalues corresponding to the compressional axis (negative eigenvalue $-\sigma$) and extensional axis (positive eigenvalue σ). Thus the sign of the production of tracer gradients by stirring depends on the angle ζ between the tracer gradient $\boldsymbol{q}$ and the compressional axis of the strain-rate tensor $\boldsymbol{S}$: $-\boldsymbol{q}^T\boldsymbol{S}\boldsymbol{q} = \sigma\boldsymbol{q}^2\cos 2\zeta$. If this angle ζ is less than 45°, there will be production of gradients (positive right-hand side of (2.15)), and vice versa. In a stationary state, the space–time average balance between the production of gradients by stirring and their destruction by diffusion implies a preferential alignment of the tracer gradient with the compressional axis, which is indeed observed in (Protas *et al.* 1999). In more detail, it can be shown that the evolution of ζ itself results from the competition between stretching and rotation (Weiss 1991) or stretching and effective rotation (Lapeyre *et al.* 1999; Klein *et al.* 2000). This competition divides the flow into elliptic regions, where the gradients do not grow, and hyperbolic regions, where ζ tends to be smaller than 45° and gradients do grow.

The picture emerging from these studies is that a tracer field initially decorrelated from the velocity field becomes deformed in such a way that geometrical alignment properties arise and strong gradients are produced. This cascade process is essentially advective, geometric (anisotropic), local and inhomogeneous in real space, due to the presence and persistence of qualitatively different hyperbolic and elliptic domains. Its magnitude and direction are determined locally by the production term (2.15). It is not very surprising to find that the approaches based on gradients and increments match at small scales. Relation (2.13) stresses the importance of the production rate of tracer gradients as a simple local indicator of the cascade. While the latter is relevant at the smallest scales reached by the cascade (the diffusive scale), the local flux $F(\boldsymbol{x}, l)$ is relevant at any given scale l, and especially at convective scales identified by relation (2.12).

2.3. *Numerical experiment*

We now discuss numerically the local flux of variance observed in a large-scale-forced statistically stationary experiment at resolution 1024^2 containing in addition to vorticity one passive tracer, both forced at wavenumber $k_I = 4$ (see Appendix B for details). The corresponding injection scale is $l_I = \pi/4$ or 128 grid scales. The flow is characterized by coherent vortices whose scale is roughly the forcing scale. We compute the local fluxes $F(\boldsymbol{x}, l)$ defined by equation (2.9). Yaglom's equation (2.12) enables to estimate the range of convective scales. A scale l of 8 grid scales is found to be convective. We discuss the statistical distribution of the transfers $F(\boldsymbol{x}, l)$ for this scale and their spatial distribution.

The distribution of the values taken by the flux $F(\boldsymbol{x}, l)$ for the convective scale l ($l/l_I = 8/128 = 0.06$) is presented in figure 1. We observe that the average direction

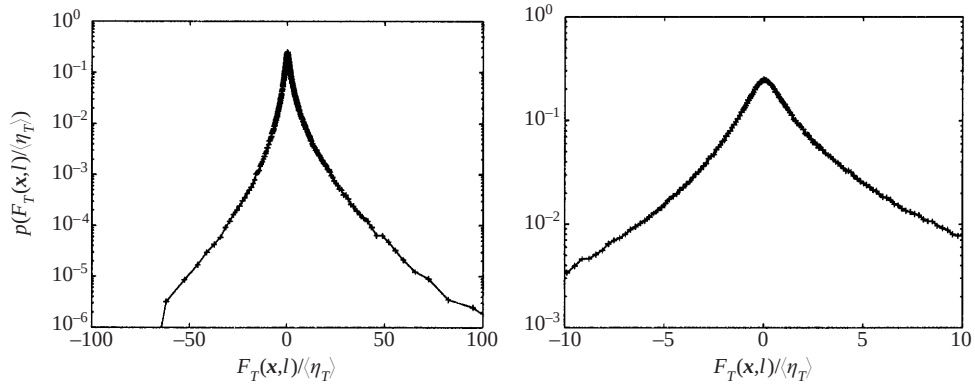

FIGURE 1. Probability distribution of the flux $F(\boldsymbol{x}, l)$ reduced by the average dissipation $\langle\eta_T\rangle_x$, for a convective scale l of 8 grid steps.

of the cascade towards small scale results from cancellations between both direct and inverse fluxes whose amplitude is large compared to the average flux $\langle F(\boldsymbol{x}, l)\rangle_x \approx \langle\eta_T\rangle_x$. The positive average results from a small asymmetry in favour of direct transfers.

The fields of passive tracer and local flux $F(\boldsymbol{x}, l)$ are displayed in figure 2. We focus on a 300×400 region containing a pair of vortices. The local flux takes either positive (direct cascade) or negative (inverse cascade) values and its amplitude can greatly exceed its spatial average $\langle F(\boldsymbol{x}, l)\rangle_x \approx \langle\eta_T\rangle_x = 147$. We can here distinguish between two types of regions:

(i) The inner part of the vortices is divided into four quarters where the cascade is alternatively direct and inverse. This quadrupolar structure is typical of elliptical vortices (Kimura & Herring 2001). Inside a vortex, fluid elements follow quasi-elliptic trajectories along which the net budget of the cascade is practically zero.

(ii) Outside the vortices, the tracer field consists of long filaments either stretched or folded by the flow. The cascade is mostly direct ($F(\boldsymbol{x}, l) > 0$) but is sometimes reversed. To interpret this reversal, we plotted on the same graph the compressional direction of the strain-rate tensor $\boldsymbol{S}$. In the regions of direct cascade, filaments are being formed by this compression and thus orthogonal to the compressional direction. Conversely, the filaments in inverse cascade zones (centre of figure 2 for instance) are parallel to the compressional axis. Thus these zones, rather, correspond to a folding of the filaments.

3. Tracer cascade and the modelling of the turbulent 'mixing'

The important distinction between stirring and mixing is based on the reversibility of the processes. Stirring deals with the convective term of equation (2.4) and is a formally reversible process that conserves the total tracer variance. Mixing on the other hand is the irreversible process by which the tracer becomes homogenized, resulting in a decrease of its variance. This is represented by the molecular diffusivity κ in the advection–diffusion equation (2.4). However, both processes are intimately linked. Pure diffusion in the absence of advection homogenizes the tracer very slowly and inefficiently, and is considerably enhanced under strong stirring. Conversely, a process analogous to mixing takes place when limitations due to resolution come into play. Let us suppose that we are dealing with limited information from which small

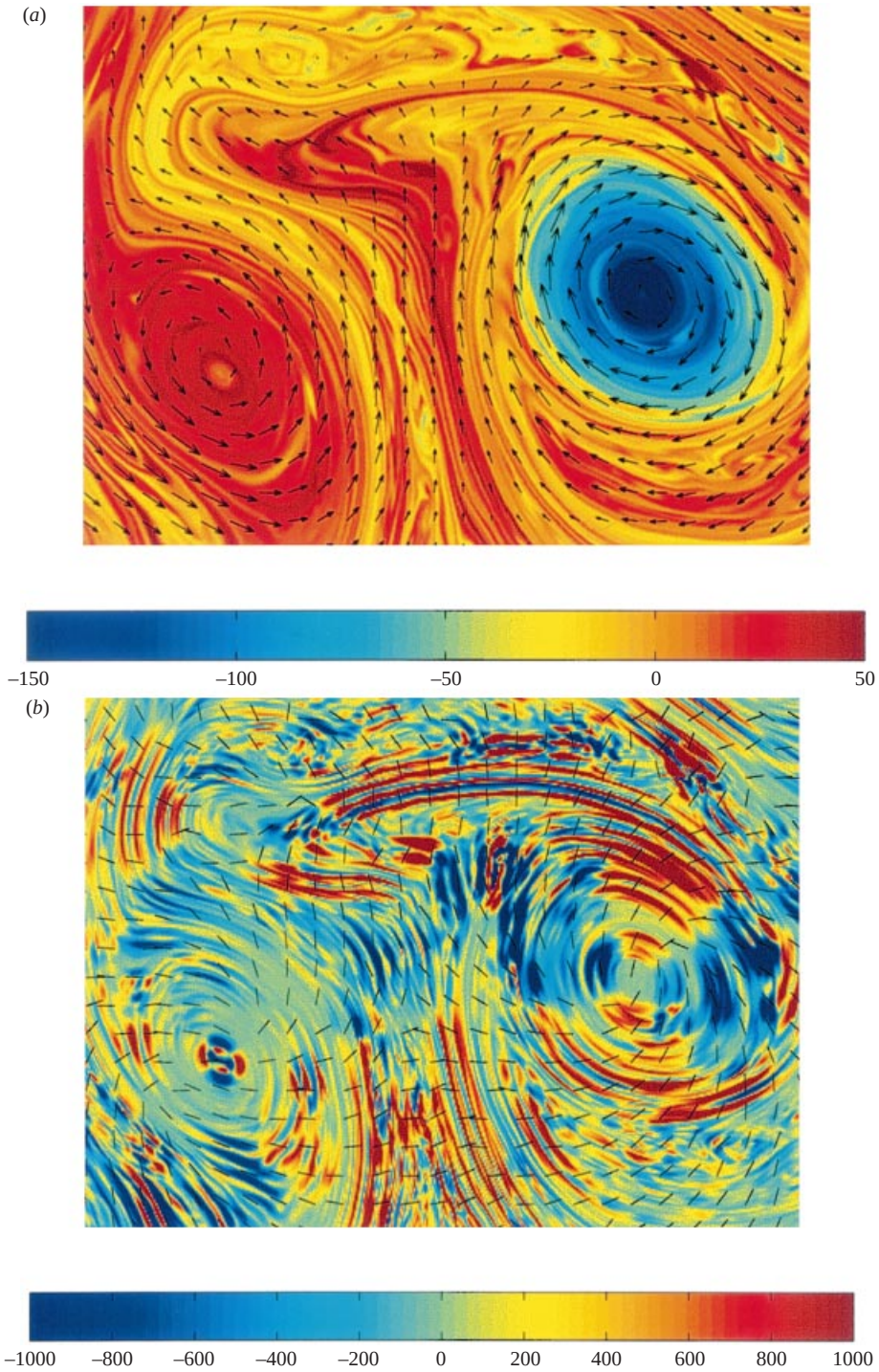

FIGURE 2. (*a*) Passive tracer and velocity (arrows) in a stationary, large-scale forced simulation. (*b*) Corresponding transfers of variance computed for a scale l of 8 grid scales that belongs to the convective range. Lines indicate the compressional direction of the flow. Zoom of a 300×400 area out of a 1024^2 box.

scales have been filtered out by a spatial low-pass filter $\varphi(l)$:

$$\theta(\boldsymbol{x}, t) = \overline{T} \equiv \int T(\boldsymbol{x} + \boldsymbol{l})\varphi(l)\,\mathrm{d}\boldsymbol{l}, \tag{3.1}$$

$$\boldsymbol{v}(\boldsymbol{x}, t) = \bar{\boldsymbol{u}} \equiv \int \boldsymbol{u}(\boldsymbol{x} + \boldsymbol{l})\varphi(l)\,\mathrm{d}\boldsymbol{l}. \tag{3.2}$$

Then if T obeys pure transport (equation (2.4) without forcing nor diffusion), the direct tracer cascade progressively empties the large scales of T to the benefit of its small scales, which are absent from θ. Subsequently, the variance of θ decreases at a rate approximately given by the spectral flux of tracer variance through the cutoff wavenumber k_c:

$$\frac{\mathrm{d}}{\mathrm{d}t}\int \frac{\theta^2}{2}\,\mathrm{d}\boldsymbol{x} \approx -\eta_T(k_c). \tag{3.3}$$

This decrease implies that θ does not obey a pure advection equation:

$$\frac{\partial\theta}{\partial t} + (\boldsymbol{v}\cdot\nabla)\,\theta = (\boldsymbol{v}\cdot\nabla)\,\theta - \overline{(\boldsymbol{u}\cdot\nabla)\,T} \equiv M[\theta] \neq 0. \tag{3.4}$$

Thus the right-hand side $M[\theta]$ of (3.4) must be modelled.† It is a linear operator in θ since the whole problem is linear in T and θ. Furthermore its spatial average is zero due to incompressibility.

However, the process by which the variance of θ decreases is not strictly speaking mixing. It results from the combined effect of the direct cascade and coarse graining, but does not tell us anything about the small-scale homogenization of the tracer. We will be interested here in the problem of properly modelling the right-hand side of (3.4), which we call modelling the turbulent 'mixing'.

In what follows we consider an anisotropic diffusivity, the properties of which we derive. We argue that this subgrid model should reproduce the tracer cascade not only on average as in equation (3.3) but locally in physical space. We then check this numerically and compare with usual isotropic parameterization: eddy diffusivity and hyperdiffusivity.

3.1. *Strain diffusivity*

At a basic level, one expects from a subgrid model that equation (3.3) be respected, thus following the spectral picture of a cascade directed on average towards small scales. Many models are able to cause such an average decrease of the resolved tracer variance. Popular ones are the eddy diffusivity model and the hyperdiffusivity model:

$$M_{eddy}[\theta] \equiv \nabla\cdot(\kappa_{eddy}\nabla\theta),$$

$$M_H[\theta] \equiv -\kappa^*(-\Delta)^p\theta,$$

with p the order of the hyperdiffusivity. The models M_{eddy} and M_H are not derived from first principles but based on the requirement of a global decrease of the tracer variance. It is however possible to derive a model from equations (3.1), (3.2) and (3.4) for a Gaussian filter of width l_0, $\varphi(l) = \exp(-l^2/2l_0^2)/2\pi l_0^2$. A formal procedure consists in recovering the full fields T and $\boldsymbol{u}$ from the resolved fields θ and $\boldsymbol{v}$. Using

† Notice that we are not concerned here with the modelling of unresolved processes (instabilities, wave breaking, etc.) but only with the effects of stirring.

a Taylor expansion in equations (3.1) and (3.2) one obtains

$$\theta \approx T + \frac{l_0^2}{2}\Delta T \Rightarrow T \approx \theta - \frac{l_0^2}{2}\Delta\theta, \tag{3.5}$$

$$\boldsymbol{v} \approx \boldsymbol{u} + \frac{l_0^2}{2}\Delta\boldsymbol{u} \Rightarrow \boldsymbol{u} \approx \boldsymbol{v} - \frac{l_0^2}{2}\Delta\boldsymbol{v}. \tag{3.6}$$

The evolution equation of θ is then obtained by substituting (3.5) and (3.6) in (3.4):

$$\frac{\mathrm{d}\theta}{\mathrm{d}t} + l_0^2\partial_i(\partial_j u_i \partial_j \theta) = 0. \tag{3.7}$$

This short formal deconvolution method is used in Moeleker & Leonard (2000). The derivation in Dubos (2001) is based on a more physical estimate of the effects of differential advection (velocity increments) using Taylor expansions. The resulting model M_{sd} is equivalent to using an anisotropic tensor diffusivity κ_{ij} proportional to the velocity gradient: $M_{sd}[\theta] = \nabla\cdot\left(\kappa_{ij}\partial_j\theta\right)$ with $\kappa_{ij} = -l_0^2\partial_j u_i$. Multiplying (3.7) by θ, we obtain the evolution of the resolved variance:

$$\begin{aligned}\frac{\mathrm{d}}{\mathrm{d}t}\frac{\theta^2}{2} + l_0^2\partial_i\left(\partial_j u_i \partial_j \frac{\theta^2}{2}\right) &= l_0^2\partial_i\theta\partial_i u_j\partial_j\theta \equiv -\eta_{sd} \\ &\approx -F(\boldsymbol{x}, 2l_0).\end{aligned} \tag{3.8}$$

Thus the local decrease of the tracer variance (right-hand side of equation (3.8)) is proportional to the creation rate of tracer gradients and involves the strain-rate tensor $\boldsymbol{S}$ (equation (2.15)). We shall refer to this model as *strain diffusivity*. Furthermore, we see here that the transfer of variance to smaller scales is reproduced not only globally but locally by strain diffusivity: the local decrease of tracer variance is approximately given by the local flux $F(\boldsymbol{x}, 2l_0)$, according to equation (2.13).

To summarize, the local decrease of the tracer variance given by the right-hand side of equation (3.8) is closely linked to the creation of small scales diagnosed by equation (2.15) (Dubos 2001). In this way strain diffusivity takes advantage of the geometry of the tracer and velocity fields being dissipative in hyperbolic domains (positive right-hand side of (3.8) due to the growth of the tracer gradients) and essentially conservative in elliptic domains (weak right-hand side of (3.8)). In addition it reproduces not only globally but at a fine-grained level the transfers of tracer variance induced by the turbulent cascade.

3.2. *Numerical experiment*

We study the spatial organization of, on one hand, the local transfer $F(\boldsymbol{x}, l)$ defined by equation (2.9) and, on the other hand, the tracer variance dissipation rate induced by strain diffusivity. We make a comparison with popular subgrid-scale parameterizations: isotropic diffusivity $\kappa\Delta\theta$, and iterated Laplacian $-\kappa^*(-\Delta)^p\theta$ with $p = 2, 8$.

To achieve this, we performed a numerical simulation of decaying turbulence including in addition to the vorticity field several passive tracers, each of them using one of the previously mentioned parameterizations. The numerical values of the parameters are summarized in Appendix B. All tracers have the same initial condition and the simulation is run during 40 turnover times. The large scales of the final tracer fields are close enough to each other so that a comparison can be made, while the length of the simulation ensures that the parameterization has eventually imprinted its own feedback on the small-scale structure of the tracer field. The resolution is 512^2.

Strain diffusivity is proportional to the tensor of velocity gradients $A_{ij} = \partial_j u_i$. Its symmetric part is the strain-rate tensor $\mathbf{S}$, which has two eigenvalues of opposite sign, inducing positive diffusivity along the compressional axis and negative diffusivity along the extensional axis. This negative diffusivity is a potential source of instability which we had to suppress by adding a small amount of dissipation. We used an iterated Laplacian in addition to the strain diffusivity and we checked that the additional dissipation is less that 30% the dissipation due to strain diffusivity, so that the latter is playing the major role. This point is discussed in more detail later in this paper.

The tracer variance dissipation induced by strain diffusivity is

$$\eta_{sd} = -l_0^2 \partial_i \theta \partial_i u_j \partial_j \theta.$$

The classical isotropic diffusivity has a dissipation rate

$$\eta_{eddy} = \kappa_{eddy} \|\nabla \theta\|^2.$$

Finally, for the iterated Laplacian of order p, the local dissipation rate is

$$\eta_H = \kappa_H \sum_{i_1 \dots i_p} (\partial_{i_1 \dots i_p} \theta)^2.$$

We focus in figure 3(a) on a vortex pair. The local tracer variance transfer $F(\boldsymbol{x}, l)$ for a scale l of 8 grid sizes is displayed in figure 3(b). It is found again to take both positive and negative values, while keeping a positive spatial average. It can be checked in figure 3(d) that strain diffusivity is able to reproduce fairly well these sign changes and the general organization of the transfers, while isotropic diffusivity (figure 3c), being everywhere positive, cannot. This reflects the fact that isotropic diffusivity is only connected to the presence of gradients, while strain diffusivity is connected to the local dynamical process of their growth – or decay. Figure 3(e, f) displays the analogous fields for the iterated Laplacian. In addition to being by construction everywhere positive, they show little relation with the structure of the transfers. This is not very surprising since these operators are valued not for their real space properties but for their Fourier space properties, where they extend inertial ranges. The counterpart is that their action is essentially uniform, not taking into account the dynamical contrasts of the flow.

Complementary information concerning the auxiliary diffusion

As mentioned above, we checked that the additional dissipation is globally less than 30% of the dissipation due to strain diffusivity. It is useful to make this global estimate more precise by a local analysis. We correlated the local dissipation rate induced by strain diffusivity η_{sd} on one hand and by the auxiliary hyperdiffusivity η_{aux} on the other hand (figure 4). The former, being proportional to the growth rate of the tracer gradient, is at the same time a local indicator of the cascade dynamics. The two contributions appear highly uncorrelated and η_{sd} mostly dominates η_{aux}: points for which $\eta_{aux} > |\eta_{sd}|$ represent 30% of the total and are characterized by values of η_{sd} close to 0. As complementary information that is more quantitative, we computed the conditional average of η_{aux} with respect to η_{sd}, $E(\eta_{aux} \,|\, \eta_{sd})$ (also shown on figure 4). This average behaves differently in regions where the gradients grow ($\eta_{sd} > 0$) or decay ($\eta_{sd} < 0$): it is essentially uniform in the latter region, and varies with η_{sd} when $\eta_{sd} > 0$, reaching a maximum where gradients grow fastest. This is consistent with the fact that regions of fast growing gradients are also regions of strong gradients, hence

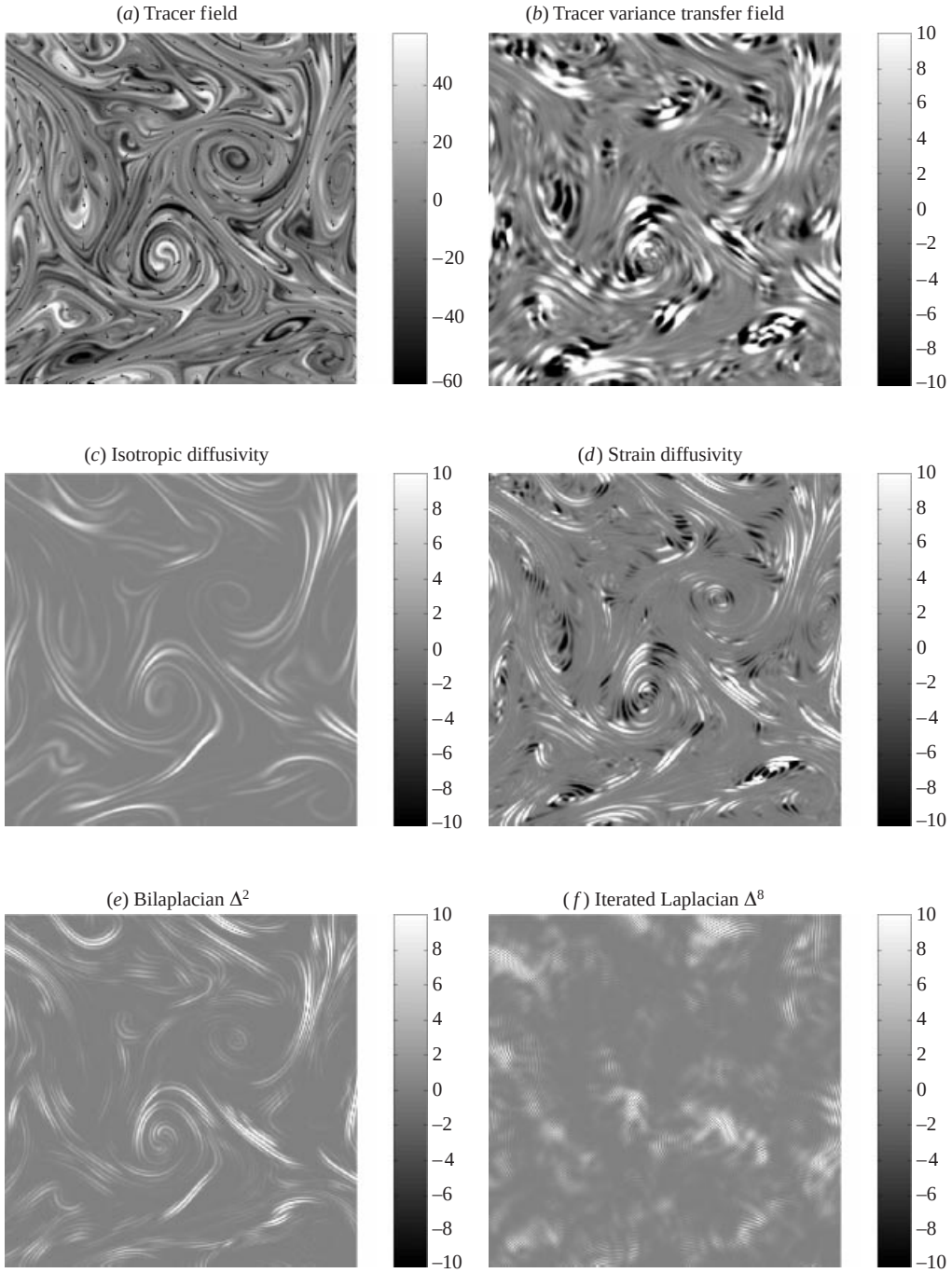

FIGURE 3. (*a*) Tracer field (zoomed) and velocity field (arrows) in a numerical simulation of freely decaying turbulence using strain diffusivity. The tracer is reduced by its root-mean-square. (*b*) Local variance transfer field $F(\boldsymbol{x}, l)$ (l is 8 grid scales). Transfers are reduced by their (positive) average value. Local transfers range from negative (locally reversed cascade) to positive (direct cascade) values. (*c–f*) Tracer variance dissipation fields $\eta_T(\boldsymbol{x})$: (*c*) isotropic diffusivity $\eta_{eddy} = \kappa \|\nabla\theta\|^2$, (*d*) strain diffusivity $\eta_{sd} = -l_0^2 \partial_i\theta\partial_i u_j \partial_j\theta$, (*e*, *f*) iterated Laplacian of order $p = 2$, $\eta_H = \sum_{ij}(\partial_{ij}\theta)^2$ (*e*) and $p = 8$, $\eta_H = \sum_{i_1 \dots i_8}(\partial_{i_1 \dots i_8}\theta)^2$ (*f*). Dissipations are reduced by their spatial averages.

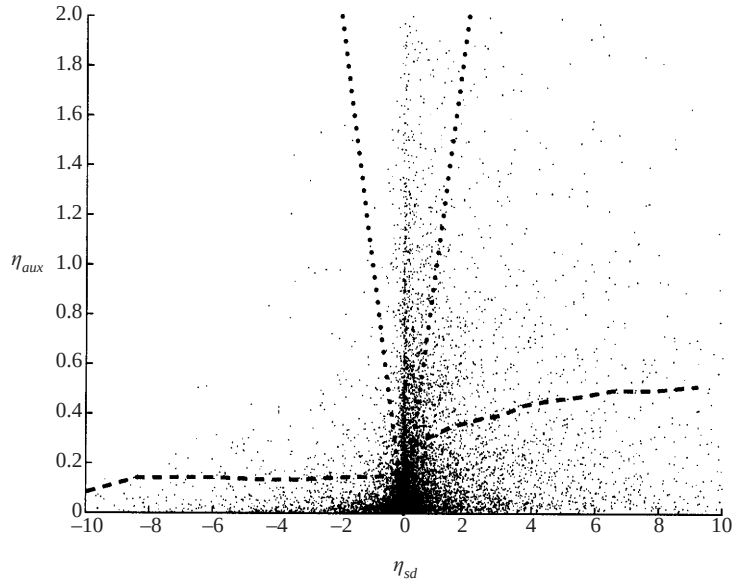

FIGURE 4. Scatter plot of dissipation produced by strain diffusivity $\eta_{sd} = -l_0^2 \partial_i \theta \partial_i u_j \partial_j \theta$ and auxiliary hyperdiffusivity η_{aux}. Dashed line: conditional average of $\eta_{aux} = \kappa_H \sum_{i_1 \dots i_p} (\partial_{i_1 \dots i_p} \theta)^2$ relative to η_{sd}. Dotted line: $\eta_{aux} = |\eta_{sd}|$. In order to compare their magnitudes, dissipations are both reduced by the spatial average of η_{sd}.

of large η_{aux}.† Finally, we computed the reciprocal conditional average $E(\eta_{sd} \,|\, \eta_{aux})$ and checked that $E(\eta_{sd} \,|\, \eta_{aux}) > 2\eta_{aux}$ except when $E(\eta_{sd} \,|\, \eta_{aux}) < 0$, which is achieved only for the smallest values of η_{aux} (not shown).

To summarize, the auxiliary diffusion is highly uncorrelated with the strain diffusivity, is dominated by it in most of the flow, and has an essentially uniform action in antidiffusive regions ($\eta_{sd} < 0$) and a slightly modulated action in the diffusive regions ($\eta_{sd} > 0$).

More sophisticated techniques may be required to suppress this instability in a more rigorous manner. One may consider completing the model with an additional diffusivity, as we did in an *ad hoc* way or based on more physical grounds. An alternative is to keep the model as is and design adapted numerical schemes, based on particles (Moeleker & Leonard 2000) or wavelets (Leonard 1997) for instance. One should be aware that these numerical schemes include implicit diffusion anyway. The situation here is that the model is obtained in a deterministic framework, e.g. including solely the (reversible) Euler equation and proper approximations. As a result, the model is formally reversible but in practice irreversible: in a turbulent flow, the global trend for tracer gradients to grow implies that strain diffusivity has a globally diffusive action ($\int \eta_{sd} \, \mathrm{d}\boldsymbol{x} > 0$) despite its reversible expression (3.7). However, the model presents a numerical instability that can be suppressed by adding either explicit or implicit diffusion as in (Laval, Dubrulle & Nazarenko 2001). The question is whether this irreversible diffusion is a fundamental part of the model representing a long-term trend (in which case it should be explicit and physically based as in Bouchet 2001) or a necessary evil stemming from numerical requirements (in which case a minimal, *ad hoc*, implicit or explicit

† This is a qualitative argument since η_{aux} is not directly connected to the tracer gradient but to higher-order derivatives.

diffusion should be best). We do not address here this question and consider that the pragmatic technique we used is sufficient for the specific goals of the present study.

4. The double cascade and the mixing of vorticity/momentum

Vorticity in two dimensions is a tracer: it is conserved along Lagrangian trajectories. But when one applies a subgrid-scale parameterization to the transport of vorticity, the velocity equation and energy budget are affected. It is of course desirable that this impact of the parameterization respect the scale-to-scale transfers of energy, which are robustly known to be towards large scales in the energy cascade range, and to vanish in the enstrophy cascade range, in the inviscid limit. Therefore it is required that the parameterization globally conserves energy. It is well known that an (eventually iterated) Laplacian always dissipates energy. Iterated Laplacians with high-order p dissipate less energy, and this is a reason why they may be preferred to a Laplacian (in addition to their capacity to extend inertial ranges). However, a small dissipation is not conservation, and attempts have been made to strictly fulfil this conservation requirement. A result is the anticipated potential vorticity method (APVM, Basdevant *et al.* 1981) which unfortunately is not frame invariant. In other words, the mixing of momentum (subgrid-scale terms for velocity) is supposed to conserve energy while the mixing of vorticity is supposed to dissipate enstrophy; of course both types of mixing are tightly connected, which makes the problem difficult. We investigate here the properties of strain diffusivity in this respect.

4.1. *Strain diffusivity and energy*

To derive the energy budget with strain diffusivity applied to vorticity, we need to know the equation for velocity corresponding to

$$\frac{\partial \omega}{\partial t} + \partial_i(v_i\omega + l_0^2 \partial_j \omega \partial_j v_i) = 0. \tag{4.1}$$

It is enough to show, following Dubos (2001), that this equation is the curl of

$$\frac{\partial v_k}{\partial t} + \partial_i(v_i v_k + l_0^2 \partial_j v_i \partial_j v_k) + \partial_k \Pi = 0, \tag{4.2}$$

with Π the coarse-grained pressure. Since $\omega = J_{kl}\partial_l v_k$ with J_{kl} the unit antisymmetric matrix, we obtain, taking the curl of equation (4.2),

$$\frac{\mathrm{d}\omega}{\mathrm{d}t} + l_0^2 \partial_i(\partial_j \omega \partial_j v_i) + J_{kl}(\partial_l v_i \partial_i v_k + l_0^2 \partial_{jl} v_i \partial_{ij} v_k) = 0. \tag{4.3}$$

Now the term $J_{kl}\partial_l v_i \partial_i v_k$ is simply the vortex stretching term which is known to vanish in two dimensions. The last term also vanishes because

$$\partial_{jl} v_i \partial_{ij} v_k = ((\partial_{xx} v_x)^2 + (\partial_{yy} v_y)^2)\delta_{kl}$$

and $J_{kl}\delta_{kl} = 0$. Thus equation (4.3) indeed reduces to (4.1) and the coarse-grained vorticity formally behaves as a passive tracer (including strain diffusivity) provided that the coarse-grained velocity also diffuses with the same space-dependent anisotropic diffusivity. This is a non-trivial result since a space-dependent diffusivity results in general in a term proportional to the diffusivity gradient in the vorticity equation. Here, both the particular expression for the diffusivity and the two-dimensionality allow such cancellations that this term vanishes. We have here a space-dependent diffusive-like operator that can be consistently applied to tracers, velocity and vorticity.

The energy budget is then obtained by multiplying equation (4.2) by v_k:

$$\frac{\partial}{\partial t}\boldsymbol{v}^2 + \partial_i(v_i\boldsymbol{v}^2 + l_0^2\partial_j v_i\partial_j(\boldsymbol{v}^2) + 2v_i\Pi) = 2l_0^2\partial_i v_k\partial_j v_k\partial_j v_i \tag{4.4}$$

but due to the two-dimensionality of the flow, we have

$$\partial_i v_k\partial_j v_i = \frac{\omega^2 - \sigma^2}{4}\delta_{jk},$$

which combined with the incompressibility constraint leads to a vanishing right-hand side in (4.4). Strain diffusivity is thus an energy-conserving, enstrophy-dissipating operator.

4.2. *Numerical experiments*

The problem of the conservation of energy is most critical in a situation where vorticity/velocity is forced at a scale close to the grid scale. Such a choice is common when one wants to study the stationary inverse energy cascade. In the case where a dissipative operator like a Laplacian or even a high-order hyperlaplacian is used, the small-scale dissipation of energy is comparable in magnitude to the spectral inverse flux of energy (Boffetta *et al.* 2000). In the high Reynolds number limit, this small-scale dissipation of energy should vanish as is observed when the forcing scale is not too close to the grid scale (see figure 6*a* below). The latter choice implies however that part of the resolution is sacrificed in order to properly resolve the enstrophy cascade.

In order to explore the possible influence of small-scale dissipation on the large scales of the flow in this context, we analyse and compare the spectral properties of the following numerical experiments (see Appendix B for details):

(i) A forced, stationary simulation at resolution 512^2, taken as a reference and labelled DNS.II as in Dubos *et al.* (2001). Energy and enstrophy are injected at wavenumber $k_I = 40$. The maximum wavenumber is $k_{max} = 230$, leaving some space for the enstrophy cascade to develop. The small-scale dissipation is a hyperdiffusivity of order $p = 8$ and the large-scale dissipation required by the inverse cascade to reach a stationary state is linear in the stream function ψ:

$$\frac{\mathrm{d}\omega}{\mathrm{d}t} + \nu^*_{512}\,\Delta^8\omega = \alpha\psi + f_\omega.$$

Typical vorticity fields of this simulation can be found in Dubos *et al.* (2001). Its spectral properties are displayed in figure 5. An acceptable energy inertial range with Kolmogorov scaling $E(k) \propto k^{-5/3}$ is found over a small decade. The poorly resolved enstrophy cascade presents a steeper slope than Kraichnan's prediction $E(k) \propto k^{-3}$.

(ii) A comparable simulation labeled 128H with a lower resolution 128^2 using the same forcing and dissipations, with the hyperviscosity coefficient ν^*_{128} tuned to fit the lower resolution:

$$\frac{\mathrm{d}\omega}{\mathrm{d}t} + \nu^*_{128}\,\Delta^8\omega = \alpha\psi + f_\omega.$$

Now the closeness between the forcing wavenumber $k_I = 40$ and the maximum wavenumber $k_{max} = 57$ raises the problem of energy dissipation.

(iii) A corresponding simulation 128SD using now strain diffusivity. As in § 3, we use an auxiliary dissipation which we choose equal to the hyperviscosity used in 128H:

$$\frac{\mathrm{d}\omega}{\mathrm{d}t} + l_0^2\partial_i\left(\partial_j\omega\partial_j v_i\right) + \nu^*_{128}\,\Delta^8\omega = \alpha\psi + f_\omega.$$

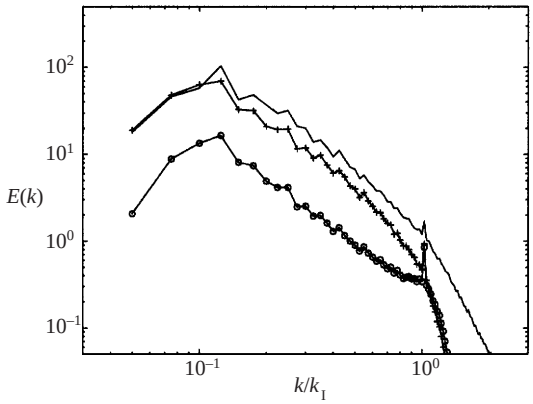

FIGURE 5. Energy spectrum $E(k)$ in experiments DNS.II (no symbol), 128H (circles) and 128SD (crosses), as a function of the reduced wavenumber k/k_I.

This choice makes the comparison more interesting, although lower values of the hyperviscosity can reduce the energy dissipation while still ensuring numerical stability.

Both simulations 128H and 128SD were initialized with a vorticity field taken from DNS.II after cutting off wavenumbers higher than $k_{max} = 57$. They were run until they reached a stationary state indicated by time-independent energy and enstrophy. For 128SD, this required about 1000 eddy turnover times $\tau \equiv Z^{-1/2}$ with Z the initial enstrophy; 30% of the energy and 50% of the enstrophy were lost during this initial stage. Simulation 128H stabilized after 3000 turnover times and lost 80% of the initial energy and enstrophy. These figures could not be reduced by tuning the hyperviscosity ν^*_{128}.

Simulations 128H and 128SD were run for 6000 turnover times. Both of them are stationary in the last 3000 and we now analyse their spectral properties averaged over this time interval. Figure 5 compares the energy spectra of the three experiments. It is clear that 128SD produces a spectrum much closer to the reference given by DNS.II than 128H does. The energy spectrum of 128H is too weak at all scales. This could be expected from the high energy dissipation induced by the hyperviscosity: the energy that is dissipated at small scales is lost for the inverse cascade and this dissipated energy is missing in the large scales of the flow. This effect still exists in 128SD but is strongly reduced.

This interpretation is confirmed by the inspection of the spectral flux of energy $\varepsilon(k)$ (figure 6*a*). The value of $\varepsilon(k)$ for $k > k_I$ is the small-scale dissipation of energy. It is weak for DNS.II, higher for 128SD, and highest for 128H. It is worth noticing that 128H and 128SD have the same hyperviscosity ν^*_{128}. We see here that SD, in addition to conserving energy itself, is able to limit the dissipation induced by the auxiliary hyperviscosity. If we examine the inverse energy flux ($\varepsilon(k)$ for $k < k_I$), it appears that the fluxes in DNS.II and 128SD are quite close to each other while the flux in 128H is much weaker. Furthermore the difference between the fluxes of 128SD and 128H is higher than the excess of dissipation present in 128H. Let us recall here that the forcing does not inject energy and enstrophy at a prescribed rate but keeps a Fourier mode constant. Thus the precise rate at which energy is injected is controlled by the dynamics. We see here that the hyperviscosity not only dissipates energy but also disturbs the dynamics enough to significantly reduce inverse energy transfers. In contrast, 128SD remains quite close to the reference DNS.II.

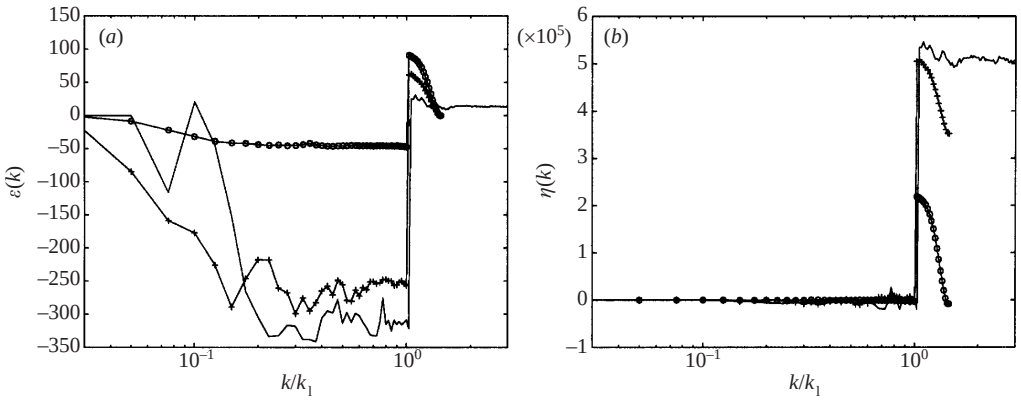

FIGURE 6. Spectral flux of (*a*) energy $\varepsilon(k)$ and (*b*) enstrophy $\eta(k)$ in experiments DNS.II (no symbol), 128H (circles) and 128SD (crosses), as a function of the reduced wavenumber k/k_I.

We finally display in figure 6(*b*) the spectral flux of enstrophy $\eta(k)$. It appears that 128SD produces an enstrophy flux close to that of DNS.II while 128H is quite different. Even by tuning ν^*_{128} a closer match cannot be obtained.

5. Discussion

In the spirit of recent results on the tracer cascade dynamics seen as a gradient enhancement process, we have studied the dynamics of tracer increments. This enabled us to consider the cascade locally in space and time, through the scale-to-scale transfers of tracer variance. The transfers give a detailed picture of the cascade, which we have discussed. It is much more complex than the average picture obtained in Fourier space. The strain diffusivity model proved to match this picture rather accurately, from analytical and numerical points of view, in contrast with isotropic models. Furthermore, it turns out that this operator can be consistently applied to tracers, velocity and vorticity, and conserves energy, in contrast with isotropic hyper/eddy diffusivities. Thus a careful modelling of enstrophy transfers allowed us in this case to obtain a good representation of energy transfers as well. This proved to have a substantial impact on the large scales of the flow in a low-resolution simulation where the enstrophy cascade is almost entirely unresolved and parametrized.

It has been shown in Rupolo *et al.* (2001) that taking into account the inhomogeneity of geophysical flows in the subgrid-scale parameterization leads to an improvement of the large-scale dynamics. What our results suggest is that a comparable improvement could be obtained by taking into account the anisotropic properties of turbulent stirring. This is probably more important for active tracers, that react with the flow, than for passive tracers. Such active tracers are ubiquitous in geophysical fluid dynamics: potential vorticity, temperature, salinity, etc. It is clear however that much remains to do. Concerning the numerical aspects of using strain diffusivity, it appears from our simulations that some efforts must be made in order to correctly implement and get advantage of it. Interesting ideas exist already for a passive tracer (Leonard 1997; Moeleker & Leonard 2000), and they should certainly be applied to vorticity. For geophysical applications, the simple framework of purely barotropic two-dimensional turbulence is insufficient and progress has to be made towards more complex situations, such as isoentropic advection in the stratosphere or isopycnal advection in the oceans.

We gratefully acknowledge Lien Hua and Claude Basdevant for their useful comments. This work was supported by the Ministère de l'Éducation Nationale, de la Recherche et de la Technologie (A.C.I. *jeunes chercheurs* 0693) and by IDRIS, project 940338.

Appendix A. Increment dynamics with forcing and diffusion

We now consider a forced and diffused tracer obeying equation (2.4). We obtain for the tracer increment:

$$\left(\frac{\partial}{\partial t} + \boldsymbol{u}^{\pm}\cdot\nabla - \kappa\Delta\right) T^{\pm} = f_T^{\pm},$$

$$\left(\frac{\partial}{\partial t} + \boldsymbol{U}\cdot\nabla - \kappa\Delta\right) \delta T = -\frac{\delta\boldsymbol{u}}{2}\cdot\nabla(T^{+}+T^{-}) + \delta f_T,$$

$$\left(\frac{\partial}{\partial t} + \boldsymbol{U}\cdot\nabla_x + \delta\boldsymbol{u}\cdot\nabla_l\right) \frac{\delta T^2}{2} = \delta T\,\Delta_x\delta T + \delta T\delta f_T.$$

We now have to rewrite $\delta T\Delta_x\delta T$ in a suitable form splitting space and scale contributions. We have, using $2\nabla_l T^{\pm} = \pm\nabla_x T^{\pm}$,

$$\begin{aligned}
2\,\Delta_l\delta T^2 &= T^{+}\Delta_x T^{+} + T^{-}\Delta_x T^{-} - T^{+}\Delta_x T^{-} - T^{-}\Delta_x T^{+} \\
&\qquad +2\nabla_x T^{+}\cdot\nabla_x T^{-} + \|\nabla_x T^{+}\|^2 + \|\nabla_x T^{-}\|^2, \\
\tfrac{1}{2}\Delta_x\delta T^2 &= T^{+}\Delta_x T^{+} + T^{-}\Delta_x T^{-} - T^{+}\Delta_x T^{-} - T^{-}\Delta_x T^{+} \\
&\qquad -2\nabla_x T^{+}\cdot\nabla_x T^{-} + \|\nabla_x T^{+}\|^2 + \|\nabla_x T^{-}\|^2, \\
\delta T\Delta_x\delta T &= T^{+}\Delta_x T^{+} + T^{-}\Delta_x T^{-} - T^{+}\Delta_x T^{-} - T^{-}\Delta_x T^{+} \\
&= (\tfrac{1}{4}\Delta_x + \Delta_l)\delta T^2 - (\|\nabla_x T^{+}\|^2 + \|\nabla_x T^{-}\|^2).
\end{aligned}$$

Collecting terms we obtain equation (2.10). It is actually possible to obtain an analogous equation for any moment of δT. Using Newton's binomial formula and similar arguments, we obtain

$$\begin{aligned}
&\left(\frac{\partial}{\partial t} + \boldsymbol{U}\cdot\nabla_x + \delta\boldsymbol{u}\cdot\nabla_l - \kappa(\tfrac{1}{2}\Delta_x + 2\,\Delta_l)\right)\frac{\delta T^n}{n} \\
&\qquad = \delta T^{n-1}\delta f_T - (n-1)\delta T^{n-2}(\eta^{+}+\eta^{-}).
\end{aligned}$$

Appendix B. Numerical parameters

The parameters used in the numerical simulations presented in the paper are summarized in table 1. The equilibrium values (§§ 2 and 4) or initial values (§ 3) of energy E and enstrophy Z are provided as complementary information.

We use a pseudo-spectral code with doubly periodic boundary conditions and leapfrog (second-order) time stepping. The simulations discussed have resolution $N \times N$ corresponding to a grid size $\Delta l = 2\pi/N$ and maximum wavenumber k_{max}. The small-scale dissipation can be (possibly iterated) Laplacian with hyperviscosity/hyperdiffusivity ν^{*}/κ^{*} used alone or together with strain diffusivity with cutoff scale l_0, expressed here in multiples of the grid size Δl. The eventual forcing is achieved by keeping the Fourier mode for the wavenumber $\boldsymbol{k}_I = (0, k_I)$ constant, corresponding

Section	Field	N	k_{max}	Δt	$l_0/\Delta x$	p	ν^*, κ^*	α	k_I	E	Z
2	ω, T	1024	460	1×10^{-4}		1	50	1	4	16.9	213
3	ω	512	170	2×10^{-4}		1	40			1.3	90
	θ_{eddy}					1	30				
	θ_{sd}				1	8	50				
	θ_{H2}					2	30				
	θ_{H8}					8	50				
4	DNS.II	512	230	2.5×10^{-5}		8	2.8×10^4	7	40	750	11×10^4
	128H	128	57	1×10^{-4}		8	1000	7	40	100	2×10^4
	128SD	128	57	1×10^{-4}	0.5	8	1000	7	40	450	5×10^4

TABLE 1. Numerical parameters.

to an injection scale $l_I = \pi/k_I = \Delta l N/2k_I$. A large-scale energy sink is then present in the form of a term proportional to the stream function $\psi = -\Delta^{-1}\omega$ added into the vorticity equation:

$$\frac{\partial \omega}{\partial t} + \nabla \cdot (\boldsymbol{u}\omega + l_0^2 \nabla \boldsymbol{u} \nabla \omega) = \alpha \Delta^{-1} \omega - \nu^* k_{max}^{-2p} (-\Delta)^p \omega + f_\omega,$$

$$\frac{\partial T}{\partial t} + \nabla \cdot \left(\boldsymbol{u}T + l_0^2 \nabla \boldsymbol{u} \nabla T\right) = \alpha \Delta^{-1} T - \kappa^* k_{max}^{-2p} (-\Delta)^p T + f_T.$$

The use of strain diffusivity adds in this spectral scheme a computational cost of roughly 50%, comparable to the cost of Smagorinsky's model. This cost is probably lower in real-space-based schemes like finite elements or finite volume methods.

REFERENCES

BABIANO, A., BASDEVANT, C. & SADOURNY, R. 1985 Structure functions and dispersion laws in two-dimensional turbulence. *J. Atmos. Sci.* **42**, 941–949.

BASDEVANT, C., LEGRAS, B., SADOURNY, R. & BELAND, M. 1981 A study of barotropic model flows: intermittency waves and predictability. *J. Atmos. Sci.* **38**, 2305–2326.

BASDEVANT, C. & PHILIPOVITCH, T. 1994 On the validity of the "Weiss criterion" in two-dimensional turbulence. *Physica* D **73**, 17–30.

BATCHELOR, G. K. 1959 Small-scale variation of convected quantities like temperature in turbulent fluid. *J. Fluid Mech.* **5**, 113–133.

BOFFETTA, G., CELANI, A. & VERGASSOLA, M. 2000 Inverse cascade in two-dimensional turbulence: deviations from Gaussianity. *Phys. Rev.* E **61**, R29–R32.

BOUCHET, F. 2001 Mécanique statistique pour des écoulements géophysiques. PhD thesis, Université Joseph Fourier, Grenoble.

CORRSIN, S. 1951 On the spectrum of isotropic temperature fluctuations in an isotropic turbulence. *J. Appl. Phys.* **22**, 469–473.

CRISANTI, A., FALCONI, M., PALADIN, G. & VULPIANI, A. 1990 Role of Lagrangian chaoticity on the small scale structure of passive scalars in fluids. *Physica* A **166**, 305–324.

DUBOS, T. 2001 A spatially selective parameterization for the transport of a passive or active tracer by a large scale flow. *C. R. Acad Sci. Paris* **329**, 509–516.

DUBOS, T., BABIANO, A., PARET, J. & TABELING, P. 2001 Intermittency and coherent structures in the two-dimensional inverse energy cascade: comparing numerical and laboratory experiments. *Phys. Rev.* E **64**, art. no. 036302.

HUA, B. & KLEIN, P. 1998 An exact criterion for the stirring properties of nearly two-dimensional turbulence. *Physica* D **113**, 98–110.

KIMURA, Y. & HERRING, J. 2001 Gradient enhancement and filament ejection for non-uniform elliptic vortex in two-dimensional turbulence. *J. Fluid Mech.* **439**, 43–56.

Klein, P., Hua, B. L. & Lapeyre, G. 2000 Alignment of tracer gradients in two-dimensional turbulence using second order Lagrangian dynamics. *Physica* D **146**, 246–260.

Kraichnan, R. 1967 Inertial ranges in two-dimensional turbulence. *Phys. Fluids.* **10**, 1417–1423.

Kraichnan, R. 1971 Inertial-range transfer in two- and three-dimensional turbulence. *J. Fluid Mech.* **47**, 525–535.

Lapeyre, G., Klein, P. & Hua, B. L. 1999 Does the tracer gradient align with the strain eigenvectors in 2d turbulence? *Phys. Fluids* **11**, 3729–3737.

Laval, J.-P., Dubrulle, B. & Nazarenko, S. 2001 Fast numerical simulations of 2D turbulence using a dynamic model for subgrid motions. Preprint.

Leonard, A. 2000 Large-eddy simulation of chaotic convection and beyond. *AIAA Paper* 97-0204.

Moeleker, P. & Leonard, A. 2000 Lagrangian methods for the tensor-diffusivity subgrid model. *Advances in Turbulence VIII* (ed. C. Dopazo), pp. 599–602. CIMNE, Barcelona.

Monin, S. & Yaglom, A. 1971 *Statistical Fluid Mechanics.* MIT Press.

Obukhov, A. 1949 Structure of the temperature field in turbulent flows. *Izv. Akad. Nauk. SSSR* **13**, (1) 58–69.

Paret, J. & Tabeling, P. 1997 Experimental observation of the two-dimensional inverse energy cascade. *Phys. Rev. Lett.* **79**, 4162.

Pedlosky, J. 1979 *Geophysical Fluid Dynamics.* Springer.

Protas, B., Babiano, A. & Kevlahan, N. K.-R. 1999 On geometrical alignment properties of two-dimensional forced turbulence. *Physica* D **128**, 169–179.

Rhines, P. 1979 Geostrophic turbulence. *Annu. Rev. Fluid Mech.* **11**, 401–441.

Rupolo, V., Babiano, A., Artale, V. & Iudicone, D. 2001 Horizontal space-time dependent tracer diffusivity field for an OGCM: a sensivity study in the Mediterranean Sea. *J. Mar. Res.* (submitted).

Smagorinsky, J. 1963 General circulation experiments with the primitive equations. *Mon. Wea. Rev.* **91**, 99–164.

Weiss, J. 1991 The dynamics of enstrophy transfer in two-dimensional turbulence. *Physica* D **48**, 273–294.

Yaglom, A. M. 1949 On the local structure of temperature field in turbulent flow. *Dokl. Akad. Nauk. USSR* **69**(6), 743–746.